# Electrochemical Reduction of [Ni(Mebpy)<sub>3</sub>]<sup>2+</sup>. Elucidation of the Redox Mechanism by Cyclic Voltammetry and Steady-State Voltammetry in Low Ionic Strength Solutions.

Dr. Koushik Barman, Prof. Martin A. Edwards, Prof. David P. Hickey, Dr. Christopher Sandford, Prof. Yinghua Qiu, Dr. Rui Gao, Prof. Shelley D. Minteer\*, and Prof. Henry S. White\*

Department of Chemistry, University of Utah, 315 South 1400 East, Salt Lake City, Utah 84112-0850, United States

**Abstract**. Bipyridine complexes of Ni are used as catalysts in a variety of reductive transformations. Here, the electroreduction of  $[Ni(Mebpy)_3]^{2+}$  (Mebpy = 4,4'-dimethyl-2,2'-bipyridine) in dimethylformamide is reported, with the aim of determining the redox mechanism and oxidation states of products formed under well-controlled electrochemical conditions. Results from cyclic voltammetry, steady-state voltammetry (SSV) and chronoamperometry demonstrate that  $[Ni(Mebpy)_3]^{2+}$  undergoes two sequential 1e reductions at closely separated potentials  $(E^{0'}_1 = -1.06 \pm 0.01 \text{ V})$  and  $E^{0'}_2 = -1.15 \pm 0.01 \text{ V}$  vs Ag/AgCl (3.4 M KCl)). Homogeneous comproportionation to generate  $[Ni(Mebpy)_3]^+$  is demonstrated in SSV experiments in low ionic strength solutions. The comproportionation rate constant is determined to be >  $10^6 \text{ M}^{-1}\text{s}^{-1}$ , consistent with rapid outer-sphere electron transfer. Consequentially, on voltammetric time scales, the 2e reduction of  $[Ni(Mebpy)_3]^{2+}$  results in formation of  $[Ni(Mebpy)_3]^{1+}$  as the predominant species released into bulk solution. We also demonstrate that  $[Ni(Mebpy)_3]^0$  slowly loses a Mebpy ligand (~10 s<sup>-1</sup>).

Keywords: Cyclic Voltammetry, Reaction Mechanism, Molecular electrochemistry, Computational chemistry, Nickel, Transition metals, Voltammetry

<sup>\*</sup> minteer@chem.utah.edu; white@chem.utah.edu

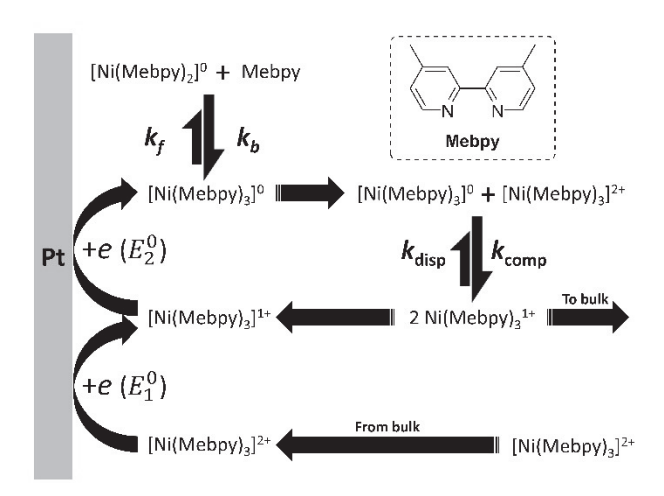
#### Introduction

Nickel-based molecular electrocatalysts have been extensively studied for a variety of reductive reactions ranging from  $H_2$  evolution<sup>[1,2]</sup> and  $CO_2$  reduction<sup>[3,4]</sup> to reductive cross-coupling in the formation of complex carbon skeletons. <sup>[5,6,7]</sup> Such catalysts commonly utilize an electrochemical reduction step to generate a reactive oxidation state of the Ni complex from which the catalytic cycle is initiated. However, experimental methods to determine the exact nature, and mechanism of reactivity, of the catalytically active Ni complex are often restricted by the short time scales of its existence within a catalytic reaction mixture.

Of specific interest to our current research, a Ni(II) 4,4'-dimethyl-2,2'-bipyridine complex,  $[Ni(Mebpy)_3]^{2+}$ , has been recently reported as a catalyst for electrochemically-driven aryl amination reactions. During this process,  $[Ni(Mebpy)_3]^{2+}$  is reduced, under a constant applied current, yielding a catalytically active Ni species in the bulk solution, which has yet to be identified. During the past three decades, the reduction of tris(bipyridine)Ni(II) complexes have been extensively investigated, with conflicting conclusions reported in the literature. While it is clear that  $[Ni(bpy)_3]^{2+}$  (bpy = 2,2'-bipyridine) can undergo multiple reductions in non-aqueous solvents, e.g., acetonitrile<sup>[8]</sup>, there are discrepancies in the interpretation of voltammetric and polarographic results. Both 1e and 2e reductions of  $[Ni(bpy)_3]^{2+}$ , yielding  $[Ni(bpy)_3]^+$  and  $[Ni(bpy)_3]^0$ , respectively, have been reported as the initial electrochemical step in acetonitrile. Apply  $[Ni(bpy)_3]^0$ , some reports suggest that  $[Ni(bpy)_3]^{2+}$  and  $[Ni(bpy)_3]^0$  undergo comproportionation to generate  $[Ni(bpy)_3]^{1+}$ ,  $[Ni(bpy)_3]^0$ , is unstable and loses a bpy ligand.  $[Ni(bpy)_3]^0$ . The overall mechanistic possibilities based on literature reports are shown in Scheme 1. To the best

of our knowledge, none of these mechanisms have been quantitatively investigated, including measurement of the formal redox potentials  $[Ni(Mebpy)_3]^{2+/+}$  and  $[Ni(Mebpy)_3]^{+/0}$  ( $E_1^{0'}$  and  $E_2^{0'}$  respectively in Scheme 1).

Herein, we report a detailed electrochemical investigation, in the absence of a catalytic substrate, aimed at fully characterizing the underlying mechanistic pathways that follow the initial 2e reduction of  $[Ni(Mebpy)_3]^{2+}$  in dry DMF solutions. Because of the complexity of the competing heterogeneous and homogeneous reactions shown in Scheme 1, the elucidation of mechanistic details required multiple electrochemical methods. We have employed both transient (cyclic voltammetry and chronoamperometry) and steady-state (ultramicroelectrode, UME) voltammetry methods, in combination with numerical simulations of transport and reactions to provide a complete description of the overall 2e reduction of  $[Ni(Mebpy)_3]^{2+}$ . Our investigations yield a number of previously unreported parameters, including the thermodynamic potentials of the first and second 1e steps  $(E_1^{0'}$  and  $E_2^{0'}$ ) of  $[Ni(Mebpy)_3]^{2+}$  reduction, the equilibrium constant and rate of ligand loss  $(k_f)$  from  $[Ni(Mebpy)_3]^0$ , and the rate of comproportionation  $(k_{Comp})$  between  $[Ni(Mebpy)_3]^{2+}$  and  $[Ni(Mebpy)_3]^0$ .



**Scheme 1.** Sequential two 1*e* electroreduction steps of  $[Ni(Mebpy)_3]^{2+}$  coupled to comproportionation and loss of ligand from  $[Ni(Mebpy)_3]^0$ .

## **Experimental**

Chemicals. All reagents were purchased from Sigma-Aldrich. Prior to electrochemical measurements, DMF was first dried overnight over activated 4 Å molecular sieves. Ni[(Mebpy)<sub>3</sub>]<sup>2+</sup> was prepared "in-situ" in the electrochemical cell by mixing 1 equiv. of NiBr<sub>2</sub>.3H<sub>2</sub>O with 6 equiv. of 4,4'-dimethyl-2,2'-bipyridine (Mebpy). Alternatively, an isolated sample of anhydrous Ni(Mebpy)<sub>3</sub>Br<sub>2</sub> was prepared by mixing 1 equiv. Of NiBr<sub>2</sub>.3H<sub>2</sub>O with 6 equiv. of Mebpy in methanol for 2 hr, collecting and washing the precipitate with methanol, and drying at room temperature. The electrochemical supporting electrolytes, (n-butyl)<sub>4</sub>ammonium hexafluorophosphate (TBAPF<sub>6</sub>) and (n-butyl)<sub>4</sub>ammonium bromide (TBABr), were recrystallized and dried.

Electrochemical measurements. Electrochemical data were recorded with a CH Instruments 760E bipotentiostat, with the electrochemical cell inside a Faraday cage. A 12.5-μm diameter Pt disk electrode (CH Instruments) was used as the working electrode in steady-state voltammetric measurements. For these measurements, a leakless Ag/AgCl (3.4 M KCl) electrode (eDAQ) was employed as a combined reference/counter electrode. A 1-mm radius Pt disk electrode, shrouded in Teflon, along with the Ag/AgCl (3.4 M KCl) reference electrode and a Pt wire counter electrode, were employed in cyclic voltammetric measurements. All measurements were performed in Ar-bubbled solutions under an Ar atmosphere and employed flame-dried glassware.

Simulations of Electrochemical Experiments. Finite-element simulations of the steady-state response of 12.5 μm-radius Pt disk electrode were performed using COMSOL Multiphysics, ver. 5.4a. Details of the simulation mesh and parameters are provided in the *Supporting Information*. Finite-difference simulations of the cyclic voltammetric response of the larger 1 mm-radius Pt disk electrode were performed using DigiSim, ver. 3.03b.

## **Results and Discussion**

We performed preliminary cyclic voltammetric (CV) experiments to examine the redox properties of  $[Ni(Mebpy)_3]^{2+}$  as prepared *in situ* in dry DMF solutions containing 0.5 mM NiBr<sub>2</sub> and 3 mM Mebpy. The 6:1 equivalent ratio of ligand to metal ions yields the  $[Ni(Mebpy)_3]^{2+}$  complex. (Experiments presented in the Supporting Information demonstrate that the CV response in DMF solutions containing Mebpy and  $[Ni(Mebpy)_3]^{2+}$  does not vary when the ligand is present in greater than a ~3:1 excess of the metal ion.)

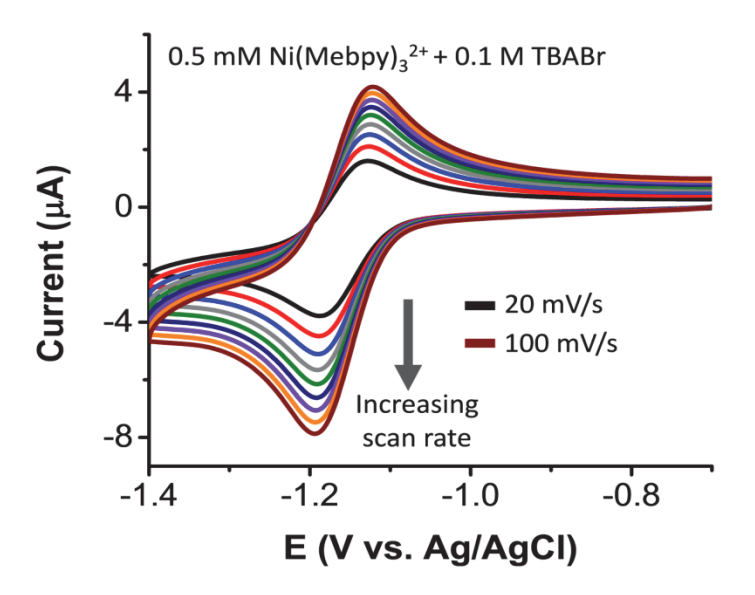


**Figure 1.** Cyclic voltammograms recorded at a 1 mm-radius Pt disk electrode in a dry DMF solution containing 0.5 mM NiBr<sub>2</sub>, 3 mM Mebpy (v = 20-100 mV/s) in the presence of 0.1 M TBABr.

Figure 1 shows the CV response recorded at a 0.03 cm<sup>2</sup> Pt disk electrode corresponding to the reduction of [Ni(Mebpy)<sub>3</sub>]<sup>2+</sup>. A single voltammetric wave is observed in the solution containing 0.5 mM [Ni(Mebpy)<sub>3</sub>]<sup>2+</sup> and 0.1 M (n-butyl)<sub>4</sub>ammonium bromide (TBABr) as the supporting electrolyte. This wave is characterized by a half-wave potential,  $E_{1/2} = -1.15$  V vs Ag/AgCl (as determined by the average value of the cathodic and anodic peak potentials,  $E_{pc}$  and  $E_{pa}$ , respectively), and a peak splitting, ( $E_{pc} - E_{pa}$ ) of 73 (+/- 3) mV (after compensation of a small ohmic ( $iR_s$ ) potential drop). A plot of the background subtracted cathodic peak current,  $i_{pc}$ , as a function of the square root of scan rate ( $v^{1/2}$ ) for v between 20 and 100 mV/s was found to be linear with a zero intercept, indicating that reduction of [Ni(Mebpy)<sub>3</sub>]<sup>2+</sup> is diffusion controlled (Figure S1). The ratio of the anodic and cathodic peak currents,  $i_{pa}/i_{pc}$ , was found to be close to unity, independent of scan rate down to the slowest scan rates examined (20 mV/s). This latter result suggests that the electrochemical transformation:

$$[Ni(Mebpy)_3]^{2+} + ne = [Ni(Mebpy)_3]^{(2-n)+}$$
 (1)

is chemically reversible on the voltammetric time scales employed here.

We also performed CV measurements on in-situ prepared [Ni(Mebpy)<sub>3</sub>]<sup>2+</sup> in DMF solutions employing 0.1 M (n-butyl)<sub>4</sub>ammonium hexafluorophosphate (TBAPF<sub>6</sub>) as the supporting electrolyte, as well as CV measurements in solutions prepared using a sample of anhydrous Ni(Mebpy)<sub>3</sub>Br<sub>2</sub>. The CV responses in these experiments are essentially identical to

those shown in Figure 1 (see Figure S2), indicating that eq (1) describes the general reduction of [Ni(Mebpy)<sub>3</sub>]<sup>2+</sup> in DMF.

The number of electrons (n) in eq (1) can be determined from the cathodic peak currents in the CV response shown in Figure 1, by employing the Randles-Sevcik equation, eq (2), assuming that the diffusivity (D) of [Ni(Mebpy)<sub>3</sub>]<sup>2+</sup> is known a priori.

$$i_{pc} = 0.4463 \, n^{3/2} FAC^* (FvD/RT)^{1/2}$$
 (2)

In eq (2), F is Faraday's constant, A is the electrode area, v is the scan rate, R is the gas constant, T is temperature, and  $C^*$  is the bulk concentration of  $[Ni(Mebpy)_3]^{2+}$ .

To determine D, we used the chronoamperometric method of Winlove<sup>[12]</sup>, Bard<sup>[13]</sup>, and coworkers, in which the transient current is recorded at a Pt disk microelectrode (12.5  $\mu$ m radius) following a potential step to potentials where [Ni(Mebpy)<sub>3</sub>]<sup>2+</sup> is reduced at the diffusion-controlled rate. This method is especially advantageous as it does not require *a priori* knowledge of either n or the concentration of [Ni(Mebpy)<sub>3</sub>]<sup>2+</sup>. The reader is referred to references 12 and 13 for method details and appropriate conditions where the analysis is valid.

Prior to the chronoamperometric analysis, steady-state voltammetry (SSV) was performed at the 12.5  $\mu$ m radius Pt disk microelectrode in the dry DMF solution containing 0.5 mM [Ni(Mebpy)<sub>3</sub>]<sup>2+</sup> and 0.1 M TBABr at a scan rate of 2 mV/s. As before, the [Ni(Mebpy)<sub>3</sub>]<sup>2+</sup> was prepared *in situ* by mixing 1 equiv. NiBr<sub>2</sub>·3H<sub>2</sub>O and 6 equiv. of Mebpy. The SSV response, Figure 2(a), shows that [Ni(Mebpy)<sub>3</sub>]<sup>2+</sup> reduction results in a quasi-sigmoidal voltammogram, with  $E_{1/2} \sim -1.14$  V vs Ag/AgCl, consistent with the  $E_{1/2}$  determined from the CV response (Figure

1). The steady-state value of the limiting current plateau,  $i_{ss} \sim 2.4$  nA, corresponds to the diffusion-limited reduction of [Ni(Mebpy)<sub>3</sub>]<sup>2+</sup>, which is described by

$$i_{ss} = 4nFDC^*a \tag{3}$$

where a is the radius of a disk-shaped UME.

Chronoamperometry was performed by stepping the potential of the 12.5  $\mu$ m radius Pt microdisk from an initial potential of -0.8 V (where no faradaic current is observed) to -1.3 V vs Ag/AgCl, corresponding to a potential on the diffusion-limited current plateau. The current response was recorded for 30 s, Figure 2(b), and a plot of i normalized to  $i_{ss}$  (i.e.,  $i/i_{ss}$ ) as a function of the reciprocal of the square root of time,  $i/i_{ss}$ , vs  $t^{-1/2}$ , was constructed, as shown in the inset of Figure 2(b).

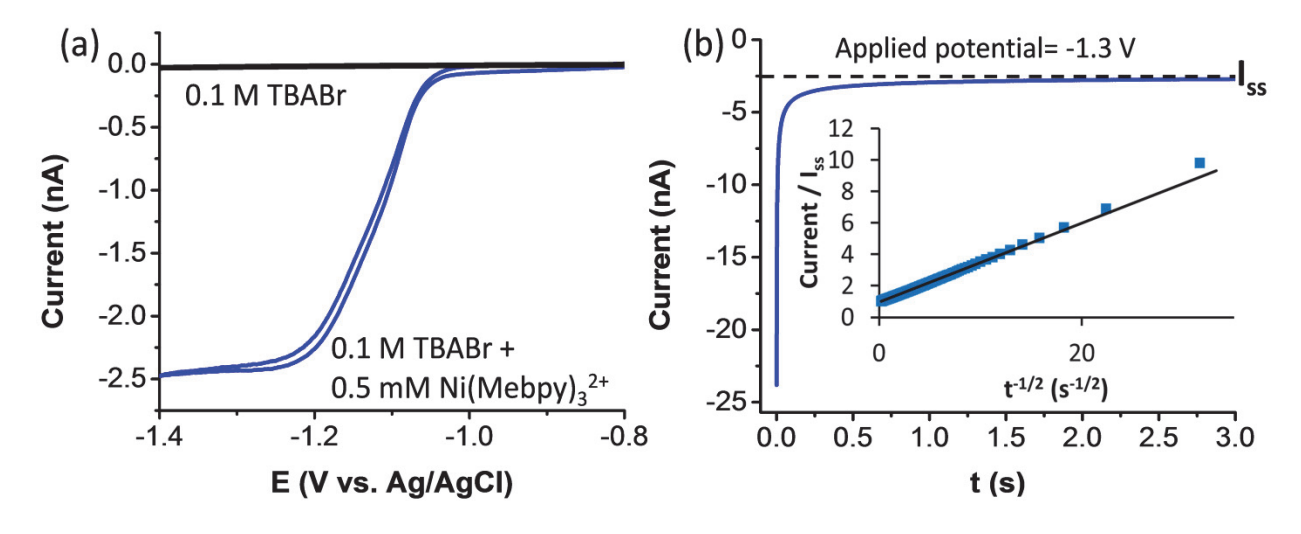


Figure 2. (a) SSV at a 12.5  $\mu$ m radius Pt disk microelectrode in the presence (blue) and absence (black) of 0.5 mM [Ni(Mebpy)<sub>3</sub>]<sup>2+</sup> at v = 2 mV/s. (b) Chronoamperometry response following a potential step from -0.8 to -1.3 V vs Ag/AgCl (first 3 s of a 30 s experiment shown). Inset shows normalized current plotted vs  $t^{-1/2}$  for full duration. The dashed line in Figure 2b shows the steady-state current value ( $i_{ss}$ ).

For a diffusion-controlled process, a plot of  $i/i_{ss}$ , vs  $t^{-1/2}$  is predicted to be linear with an intercept of unity, since  $i \to i_{ss}$  as  $t \to \infty$ . The inset of Figure 2(b) shows that the plot of  $i/i_{ss}$ , vs  $t^{-1/2}$  is indeed linear with an intercept of unity (0.97), as predicted by theory. From the slope ( $S = 0.25 \text{ s}^{1/2}$ ) of the resulting straight line, D for [Ni(Mebpy)<sub>3</sub>]<sup>2+</sup> is calculated from eq (4),

$$D = \pi a^2 / 16S^2 \tag{4}$$

Using eq (4), we compute D to be 0.5 (±0.1) x 10<sup>-5</sup> cm<sup>2</sup>/s for the data in Figure 2(b). We performed similar analysis of D in solutions containing between 1 and 10 mM [Ni(Mebpy)<sub>3</sub>]<sup>2+</sup>, and in each case, we observed linear plots of  $i/i_{ss}$ , vs t<sup>-1/2</sup> with unity intercepts; from these results, we determined an average value of D equal to 0.5 (±0.1) x 10<sup>-5</sup> cm<sup>2</sup>/s.

With D determined, the value of n may be directly computed from either  $i_{ss}$  measured in the SSV response (Figure 2(a) and eq (3)), or from  $i_{pc}$  measured in the CV response (Figure 1 and eq (2)). We determined n = 1.9 ( $\pm 0.2$ ) and 2.1 ( $\pm 0.2$ ) from the SSV and CV responses, respectively, indicating that the overall reduction of [Ni(Mebpy)<sub>3</sub>]<sup>2+</sup> is a 2e process.

Despite the finding that n=2, we note that the *shape* of the CV response shown in Figure 1 is consistent with a 1e reduction rather than a 2e reduction. Specifically, a single reversible voltammetric wave with  $\Delta E_{\rm p}$  (= $E_{\rm pc}$  -  $E_{\rm pa}$ ) ~73 mV, independent of scan rate, is suggestive of n=1. At room temperature, the theoretical value of  $\Delta E_{\rm p}$  is equal to ~58 mV for n=1, while  $\Delta E_{\rm p}$  ~29 mV for n=2. [14]

The CV response of successive two 1e reductions steps, eqs (5) and (6),

$$[Ni(Mebpy)_3]^{2+} + e = [Ni(Mebpy)_3]^{1+} E_1^{0'}$$
 (5)

$$[Ni(Mebpy)_3]^{1+} + e = [Ni(bpy)_3]^0 E_2^{0'}$$
 (6)

is expected to yield a single voltammetric wave when the difference in the formal redox potentials of the first and second steps,  $(E_1^{0'} - E_2^{0'})$ , is less than ~-100 mV, *i.e.*, when the second electron transfer occurs at a potential significantly more positive than the first, a single CV wave is expected, with  $\Delta E_p$  ~29 mV is predicted.<sup>[14]</sup> Conversely, two resolved 1e waves, each with  $\Delta E_p$  ~58 mV, are expected when  $(E_1^{0'} - E_2^{0'}) > \sim 100$  mV. We note here that the SSV response shown in Figure 2(a) displays an inflection point on the rising portion of the wave, suggestive of sequential two 1e steps with closely spaced  $E_n^{0'}$  values. We show below that the observed peak splitting of  $\Delta E_p \sim 73$  mV in the CV response for the 2e reduction of [Ni(bpy)<sub>3</sub><sup>2+</sup>], Figure 1, requires consideration of three factors: (1)  $E_2^{0'}$  being slightly negative of  $E_1^{0'}$  (as suggested by the SSV response), (2) the slow loss of Mebpy from [Ni(Mebpy)<sub>3</sub>]<sup>0</sup>, and (3) comproportionation between [Ni(Mebpy)<sub>3</sub>]<sup>2+</sup> and electrogenerated [Ni(Mebpy)<sub>3</sub>]<sup>0</sup>.

In the following section, we describe SSV measurements of  $[Ni(Mebpy)_3]^{2+}$  reduction as a function of the concentration of supporting electrolyte, as a means to determine values of  $E_1^{0'}$  and  $E_2^{0'}$  (eqs (5) and (6)). A by-product of this analysis is the measurement of the rate of comproportionation between  $[Ni(Mebpy)_3]^{2+}$  and  $[Ni(Mebpy)_3]^{0}$ . [15,16]

Steady-state voltammetry (SSV) of  $[Ni(Mebpy)_3]^{2+}$  as a function of the supporting electrolyte concentration.

Figure 3 shows SSVs recorded at a 12.5  $\mu$ m radius Pt UME corresponding to the reduction of 0.5 mM [Ni(Mebpy)<sub>3</sub>]<sup>2+</sup> in the presence and absence of 0.1 M TBABr. We observed that the steady-state limiting current in the absence of the supporting electrolyte is ~2× larger than in the presence of 0.1 M TBABr. Additionally, the SSV response in the absence of the supporting electrolyte clearly shows two closely spaced waves, corresponding to the first and second 1*e* reductions of [Ni(Mebpy)<sub>3</sub>]<sup>2+</sup>.

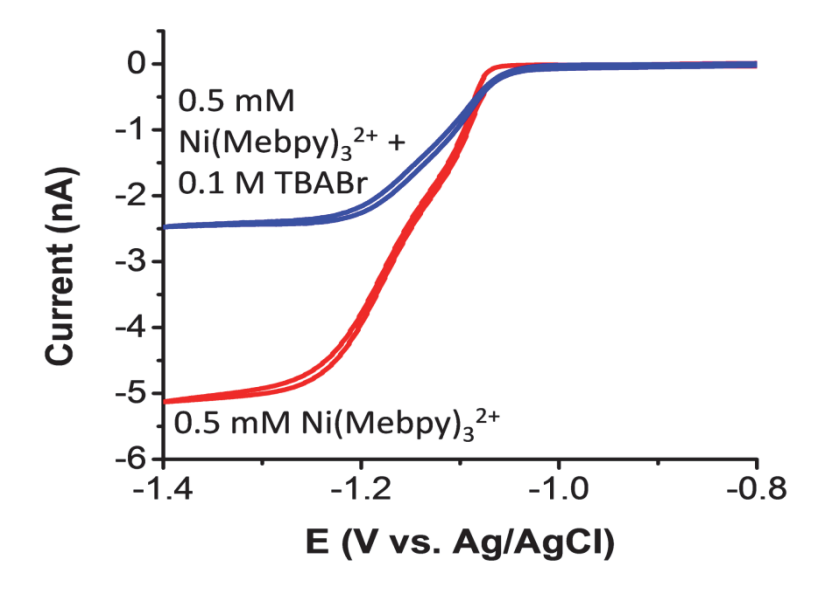


Figure 3. Steady-state voltammograms of 0.5 mM [Ni(Mebpy)<sub>3</sub>]<sup>2+</sup> at a 12.5  $\mu$ m radius Pt UME with (blue curve) and without (red curve) 0.1 M TBABr in the solution. v = 2 mV/s.

The dependence of the SSV behavior on supporting electrolyte concentration can be qualitatively understood by noting that transport of  $[Ni(Mebpy)_3]^{2+}$  to the UME in the presence of excess supporting electrolyte (TBABr: $[Ni(Mebpy)_3]^{2+}$  = 200:1) is dominated by diffusion, while both diffusion and migration contribute to transport in the absence of a supporting electrolyte. $^{[17,18]}$  For the electrochemical reduction of a positively charged species, e.g.,

 $[Ni(Mebpy)_3]^{2+}$ , the electron transfer reaction creates a small but net negative charge and electric field within the depletion layer, resulting in migration of the positive reactant *towards* the electrode surface. This migrational flux results in a larger current than observed in the presence of excess supporting electrolyte, consistent with the results in Figure 3. Conversely, for the reduction of a negatively charged species, the limiting current value will decrease due to the migration of the reactant *away* from the surface, towards the bulk solution. Similarly, the transport of an uncharged reactant will not be influenced by local electric fields.

The ~2× increase in the limiting current for  $[Ni(Mebpy)_3]^{2+}$  in the absence of TBABr is qualitatively consistent with the reduction of a 2+ species. Specifically, for a 2e reduction of a 2+ species, the limiting current is predicted to increase by precisely 3-fold based on the Amatore equation for SSV limiting currents in low ionic solutions (see *Supporting Information*). However, the difference in the enhancement of experimental (~2×) and theoretical (3×) limiting current values observed in the absence of TBABr is significant and can be attributed to the comproportionation between  $[Ni(Mebpy)_3]^{2+}$  and the 2e product,  $[Ni(Mebpy)_3]^{0+}$ , eq (7).

$$[Ni(Mebpy)_3]^{2+} + [Ni(Mebpy)_3]^0 = 2[Ni(Mebpy)_3]^{1+}$$
 (7)

Qualitatively, and described in more detail below, the comproportionation reaction results in the homogenous generation of  $[Ni(Mebpy)_3]^{1+}$  at a finite distance from the electrode surface. Reaction (7) results in a fraction of the chemically generated  $[Ni(Mebpy)_3]^{1+}$  being transported back to the electrode to undergo the second 1e reduction, while the remainder is transported

to the bulk solution. The fraction of  $[Ni(Mebpy)_3]^{1+}$  that is not reduced at the electrode, but transported back to the solution, results in the smaller increase in observed SSV limiting current (~2x) than that predicted in the absence of comproportionation (3x).

We carried out finite element simulations using COMSOL Multiphysics software to model the step-wise 2e reduction of  $[Ni(Mebpy)_3]^{2+}$  (eqs (5) and (6)) coupled to the homogenous comproportionation/disproportionation equilibrium, eq. (7). The simulations allow determination of  $E_1^{0'}$  and  $E_2^{0'}$  for the sequential electron-transfer steps, as well as the rates of comproportionation ( $k_{comp}$ ) and disproportionation ( $k_{disp}$ ). Details of the simulation process are given in the Supporting Information.

We fit the simulated SSV response to the experimental results by varying the following three parameters:  $\Delta E^{0'} = (E_1{}^{0'} - E_2{}^{0'})$ ,  $E_1{}^{0'}$ , and  $k_{\text{comp}}$ ; the simulations incorporate the measured value of D for  $[\text{Ni}(\text{Mebpy})_3]^{2+}$ . The disproportionation rate constant,  $k_{\text{disp}}$ , is uniquely determined by  $\Delta E^{0'}$  and  $k_{\text{comp}}$  through the relationships,  $\Delta E^{0'} = (\text{nF}/RT)\text{ln}(K_{\text{eq}})$  and  $K_{\text{eq}} = k_{\text{comp}}/k_{\text{disp}}$ . We assumed that the diffusivities for  $[\text{Ni}(\text{Mebpy})_3]^+$  and  $[\text{Ni}(\text{Mebpy})_3]^0$  were equal to that of  $[\text{Ni}(\text{Mebpy})_3]^{2+}$ . This assumption is likely the largest source of error in the simulation, given the dependence of D on molecular charge.

Figure 4 shows simulated SSVs of the 2e reduction 0.5 mM [Ni(Mebpy)<sub>3</sub>]<sup>2+</sup> at the 12.5  $\mu$ m radius electrode in the absence of TBABr (*Note*: Numerical convergence of the simulations requires a non-zero value of electrolyte concentration. We thus set [TBABr] =  $10^{-7}$  M in all simulations labeled as "in the absence of TBABr". However, this has no impact on the current response; see Supporting Information, Section 10 for confirmation). Figure 4(a) shows simulated SSVs obtained by varying  $k_{comp}$  between 0 and  $10^7$  M<sup>-1</sup>s<sup>-1</sup> while holding  $\Delta E^{0'}$  constant

at 90 mV ( $E_1^{0'}$  = -1.06 V,  $E_2^{0'}$  = -1.15 V vs Ag/AgCl), while Figure 4(b) shows simulated SSVs corresponding to varying  $\Delta E^{0'}$  ( $E_1^{0'}$  = -1.06 V vs Ag/AgCl was fixed while  $E_2^{0'}$  was varied) at a value of  $k_{\text{comp}}$  = 10<sup>6</sup> M<sup>-1</sup>s<sup>-1</sup>.

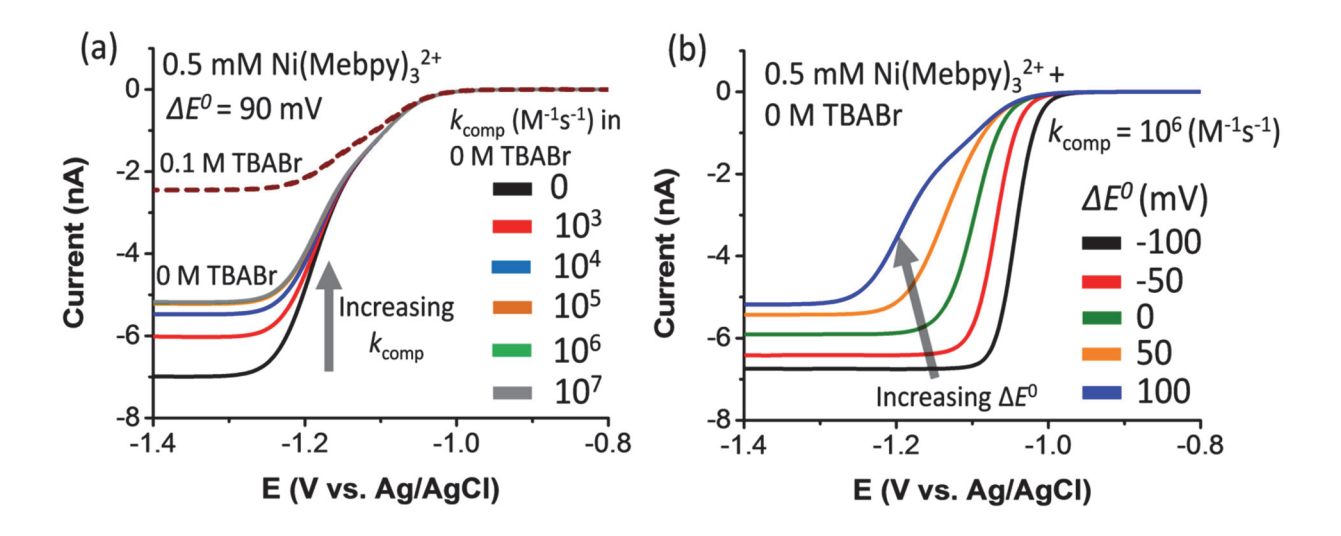


**Figure 4.** Simulated SSVs of the 2e reduction 0.5 mM [Ni(Mebpy)<sub>3</sub>]<sup>2+</sup> at a 12.5  $\mu$ m radius electrode in the absence of TBABr, (a) while varying the comproportionation rate constant ( $k_{comp}$ ) at a fixed  $\Delta E^{0'}$  ( $E_1^{0'} = -1.06 \text{ V}$ ,  $E_2^{0'} = -1.15 \text{ V}$  vs Ag/AgCl), or (b) while varying  $\Delta E^{0'}$  ( $E_1^{0'} = -1.06 \text{ V}$  vs Ag/AgCl fixed and changing  $E_2^{0'}$ ) at a fixed comproportionation rate,  $k_{comp} = 10^6 \text{ M}^{-1}\text{s}^{-1}$ . The brown dashed line in (a), shows simulated SSV response in the presence of an excess electrolyte.

We first note that the simulated SSV response in the presence of an excess electrolyte (0.1 M TBABr, brown dashed curve in Figure 4a), yields a wave that is in quantitative agreement with the experimental observation, in terms of both the magnitude of the limiting current,  $i_{\text{lim}}$ , and the  $E_{1/2}$  value. This level of agreement indicates that the finite-element model is correctly constructed. We then simulated the SSV response in the absence of TBABr, holding  $\Delta E^{0'}$  and

 $E_1^{0'}$  constant, while varying  $k_{\text{comp}}$ . We find excellent agreement between the simulated enhancement of limiting current in the absence of TBABr and the experimental value (~2×) when  $k_{\text{comp}}$  is greater than ~10<sup>6</sup> M<sup>-1</sup>s<sup>-1</sup>, while theoretically predicted<sup>16</sup> (×3) enhancement is observed when  $k_{\text{comp}} = 0$ . We then held  $k_{\text{comp}}$  constant at 10<sup>6</sup> M<sup>-1</sup>s<sup>-1</sup> and varied  $\Delta E^{0'}$  from -100 mV to 100 mV in the absence of TBABr (Figure 4b). For  $\Delta E^{0'}$  values between -100 mV and 85 mV, the simulated SSV curves show a single sigmoidal shape in the absence of TBABr. The SSV response evolves into a double wave for  $\Delta E^{0'}$  values between 90mV to 100mV without electrolyte. (Simulated SSVs with smaller changes in  $\Delta E^{0'}$  between 0 mV to 100 mV are reported in Figure S7.) In summary, the initial comparison of simulated SSV with the experimental results yields estimates of the three fitting parameters:  $k_{\text{comp}} > 10^6$  M<sup>-1</sup>s<sup>-1</sup>,  $\Delta E^{0'} \sim 90$  mV, and  $E_1^{0'} = -1.06$  V vs Ag/AgCl.

Figure 5 shows a comparison of experimental (solid) and simulated (dotted) SSVs at 2 mV/s for the reduction of 0.5 mM [Ni(Mebpy)<sub>3</sub>]<sup>2+</sup> as a function of the TBABr concentration. For TBABr concentrations between 0 and 100 mM, we obtained a very good agreement in current, potentials and wave-shape between experimental and simulated curves using the above-mentioned values of  $k_{comp}$ ,  $\Delta E^{0'}$ , and  $E_1^{0'}$ .

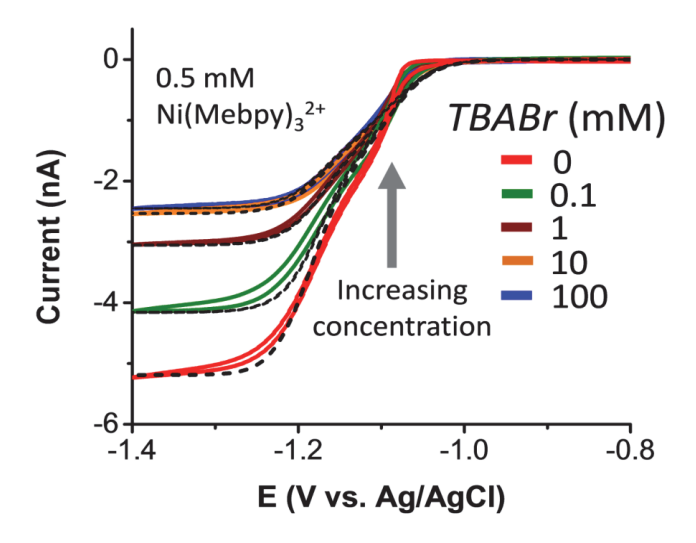


**Figure 5.** Comparison of experimental (solid) and simulated (dotted) SSVs of 0.5 mM [Ni(Mebpy)<sub>3</sub>]<sup>2+</sup> reduction with different concentrations of TBABr. 25  $\mu$ m diameter Pt disk electrode, v = 2 mV/s. Simulation details:  $k_{comp} = 10^6 \,\text{M}^{-1}\text{s}^{-1}$ ,  $\Delta E^{0'} = 90 \,\text{mV}$ , and  $E_1^{0'} = -1.06 \,\text{V}$  vs Ag/AgCl.

Figure 6 shows the simulated concentration distributions of  $[Ni(Mebpy)_3]^{2+}$ ,  $[Ni(Mebpy)_3]^{4+}$ , and  $[Ni(Mebpy)_3]^0$  resulting from the transport limited reduction of 0.5 mM  $[Ni(Mebpy)_3]^{2+}$  in the presence and absence of 0.1 M supporting electrolyte. As before, we used values of  $k_{comp} = 10^6 \, \text{M}^{-1} \text{s}^{-1}$ ,  $\Delta E^{0'} = 90 \, \text{mV}$ , and  $E_1{}^{0'} = -1.06 \, \text{V}$  vs Ag/AgCl, obtained as described above, in the simulations. In both the presence or absence of TBABr, comproportionation results in the homogeneous generation of  $[Ni(Mebpy)_3]^+$  in the solution at a fixed distance from the electrode surface, Figure 6(a) and (b), a consequence of the reaction between the  $[Ni(Mebpy)_3]^{2+}$  that is moving towards the electrode and the  $[Ni(Mebpy)_3]^0$  moving away from the electrode. In the absence of supporting electrolyte, the flux of  $[Ni(Mebpy)_3]^{2+}$  towards the electrode increases, generating a higher concentration of  $[Ni(Mebpy)_3]^0$  at the electrode surface. In turn, the higher concentration of  $[Ni(Mebpy)_3]^0$  results in an increase in the rate of comproportionation, generating additional  $[Ni(Mebpy)_3]^0$  in solution, and preventing transport of  $[Ni(Mebpy)_3]^0$  into

the solution bulk. Figure 6(d) shows a plot of the rate of comproportionation versus distance from the surface, indicating the homogeneous reaction reaches a maximum rate at ~25  $\mu$ m from the electrode surface. Additional simulations and numerical analysis show that this distance scales with the radius of the UME (a) under steady-state conditions, and is approximately equal to 2a.

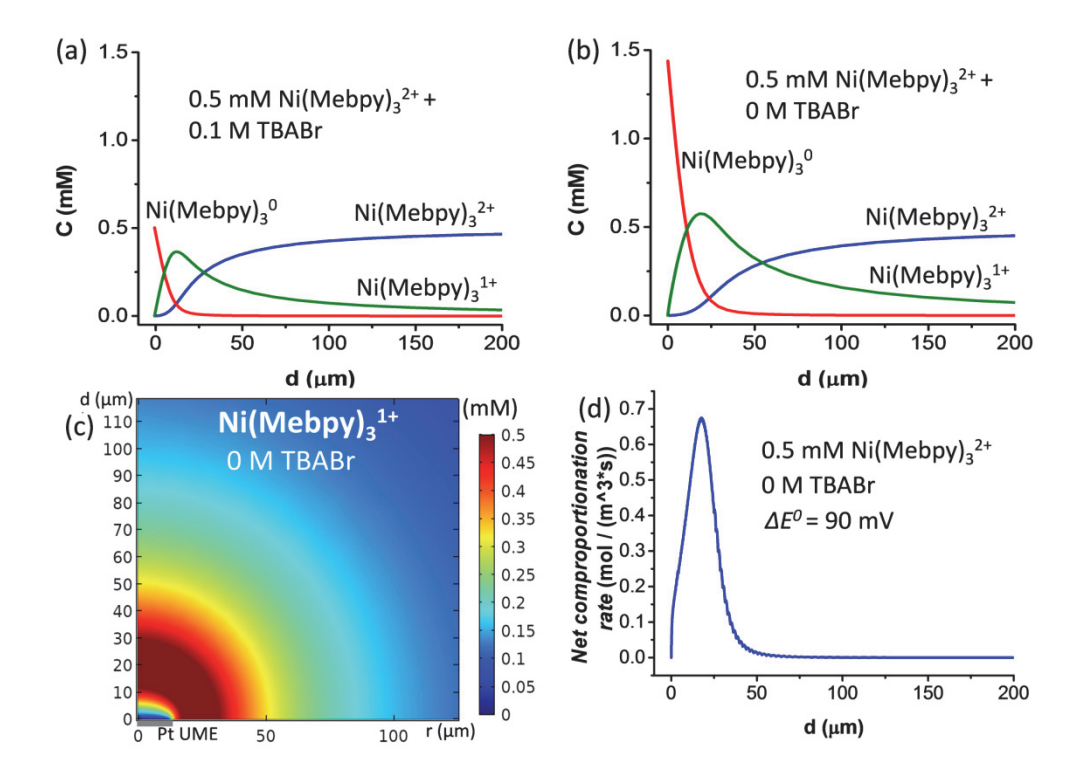


**Figure 6.** Simulated concentration profiles at potentials corresponding to the limiting current plateau (-1.3 V vs Ag/AgCl). Axial concentrations of  $[Ni(Mebpy)_3]^{2+}$ ,  $[Ni(Mebpy)_3]^{+}$ , and  $[Ni(Mebpy)_3]^{0}$  in (a) the presence of 0.1 M and (b) 0 M TBABr (d = 0 corresponds to the electrode surface). (c) Two-dimensional plot of the concentration of  $[Ni(Mebpy)_3]^{+}$  in the solution near the electrode surface. (d) Plot of the rate

of comproportionation as a function of distance from the electrode surface. In all simulations,  $k_{\text{comp}} = 10^6$  M<sup>-1</sup>s<sup>-1</sup>,  $\Delta E^{0'} = 90$  mV, and  $E_1^{0'} = -1.06$  V vs Ag/AgCl.

Effect of Mebpy Loss from  $[Ni(Mebpy)_3]^0$  on the Shape of the CV Response.

Previously, we noted that the CV response for the 2e reduction of  $[Ni(Mebpy)_3]^{2+}$  in the presence of 0.1 M TBABr exhibited a wave-shape similar to a reversible 1e process, with a splitting between cathodic and anodic peaks,  $(E_{pc} - E_{pa})$  equal to ~73 mV. Attempts to simulate this response using a finite-difference model (DigiSim) and the values of  $k_{comp} = 10^6 \, M^{-1} s^{-1}$ ,  $\Delta E^{0'} = 90 \, \text{mV}$ , and  $E_1{}^{0'} = -1.06 \, \text{V}$  vs Ag/AgCl determined from the above SSV analysis, did not provide satisfactory agreement with the experimental observations. Specifically, simulated CVs exhibited a shape corresponding to two overlapping 1e waves, a consequence of  $E_1{}^{0'}$  and  $E_2{}^{0'}$  being sufficiently separated that a single 2e wave is not realized. (Figure 12.3.24 of reference 14 shows the expected CV for this  $\Delta E^{0'}$  and provides a more detailed discussion. Figure 7, below, with K, the ligand dissociation equilibrium constant, set equal to 0, also presents the resulting CV; two overlapping waves can be clearly resolved).

Based on previous reports in the literature that indicated a loss of Mebpy from  $[Ni(Mebpy)_3]^0$ ,  $^{[8,11]}$  eq (8), we investigated the potential effect of this reaction on the CV waveshape.

$$[Ni(Mebpy)_3]^0 = [Ni(Mebpy)_2]^0 + Mebpy$$
 (8)

Figure 7 shows simulated CVs, modeled on eqs (5), (6), (7) and (8), for the 1 mm-radius Pt disk. We find good agreement between the simulated CV and the CV of Figure 1, assuming values of the forward rate constant for ligand loss,  $k_{\rm f}$ , between 9 and 20 s<sup>-1</sup>, while maintaining the equilibrium constant for eq (8), K, at 0.04 M. Note that these simulations include comproportionation with  $k_{\rm comp} = 10^6 \, {\rm M}^{-1} {\rm s}^{-1}$ , as previously determined. The simulation for  $K = 0.04 \, {\rm M}$  in Figure 7 yields a value of  $(E_{\rm pc} - E_{\rm pa})$  equal to 81 mV, in reasonable agreement with the experimental value of 73 (+/- 3) mV. We conclude that the CV wave-shape is consistent with eq (8) and previous reports of ligand loss.

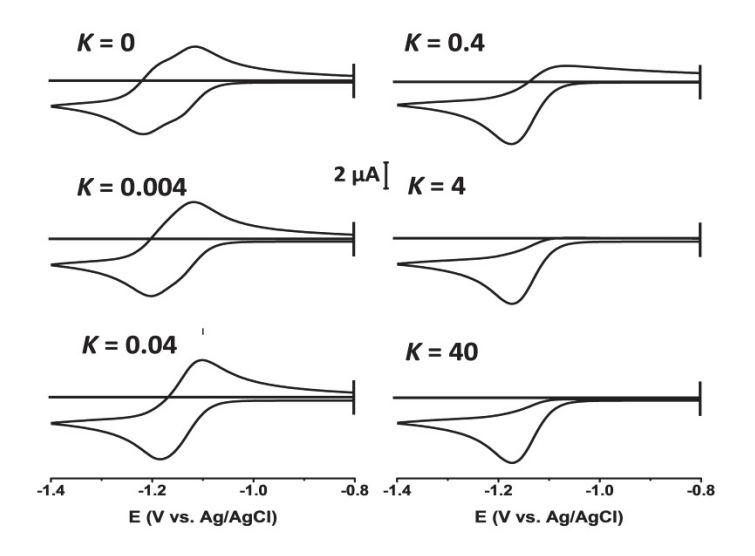


**Figure 7.** Simulated CV of 0.5 mM [Ni(Mebpy)<sub>3</sub>]<sup>2+</sup> for the 2*e* reduction process ( $E_1^{0'}$  = -1.1V vs Ag/AgCl, and  $\Delta E^{0'}$  = 90 mV) at a 1 mm-radius Pt disk electrode as a function of the ligand dissociation equilibrium constant, K (as labeled on the plots in units of M). The rate constants for ligand dissociation,  $k_f$  = 10 s<sup>-1</sup>, and comproportionation,  $k_{comp}$  = 10<sup>6</sup> M<sup>-1</sup>s<sup>-1</sup>, were held constant. v = 50 mV/s.

# Conclusion

We have demonstrated that the electroreduction of  $[Ni(Mebpy)_3]^{2+}$  in DMF occurs by two sequential 1e transfers that are accompanied by both comproportionation and slow loss of a Mebpy ligand, Scheme 1. Although these homogeneous chemical reactions have been separately suggested in previous reports, the detailed electrochemical characterization described here, in combination with computational simulations, has allowed for the first quantitative assessment of the rates of these reactions. Using SSV techniques and finite element simulations, the first two electron transfer steps have been resolved, allowing determination of the formal potentials of the  $[Ni(Mebpy)_3]^{2+/+}$  and  $[Ni(Mebpy)_3]^{4/0}$  redox couples. SSV measurements using ultramicroelectrodes in low ionic strength solutions provide an experimental means to determine a lower limit for the rate constant for comproportionation between  $[Ni(Mebpy)_3]^{2+}$  and  $[Ni(Mebpy)_3]^0$ . The measured value of  $k_{comp} \ge 10^6 \, M^{-1} s^{-1}$  suggests that this electron transfer is very facile, and is likely limited by diffusion.

Our results are relevant in understanding the recently observed catalytic activity of electroreduced  $[Ni(Mebpy)_3]^{2+}$  in electrochemically-driven aryl amination reactions. First, the fast comproportionation reaction suggests that, despite the electroreduction of  $[Ni(Mebpy)_3]^{2+}$  being a 2e process,  $[Ni(Mebpy)_3]^+$  rather than  $[Ni(Mebpy)_3]^0$  is the product species generated on voltammetric times scales, and is the predominant product in reductive electrolysis of  $[Ni(Mebpy)_3]^{2+}$  up to at least 1e per  $[Ni(Mebpy)_3]^{2+}$ .  $[Ni(Mebpy)_3]^0$  exists at significant concentrations only in close proximity to the electrode surface. Second, ligand loss is almost certainly involved in the catalytic activity of electroreduced  $[Ni(Mebpy)_3]^{2+}$  in aryl amination reactions. The estimated rate constant of ~10 s-1 for this process suggests that the loss of a ligand can free coordination sites at the nickel center for binding of the amine substrate,

enabling downstream catalytic events. Finally, with knowledge of these processes in hand, we envisage that properties of the catalyst can be systematically changed to vary both kinetic and thermodynamic values, facilitating the design of electrocatalysts which exhibit improved catalytic efficiencies.

## **Conflicts of interest**

There are no conflicts of interest to declare.

#### **Acknowledgments**

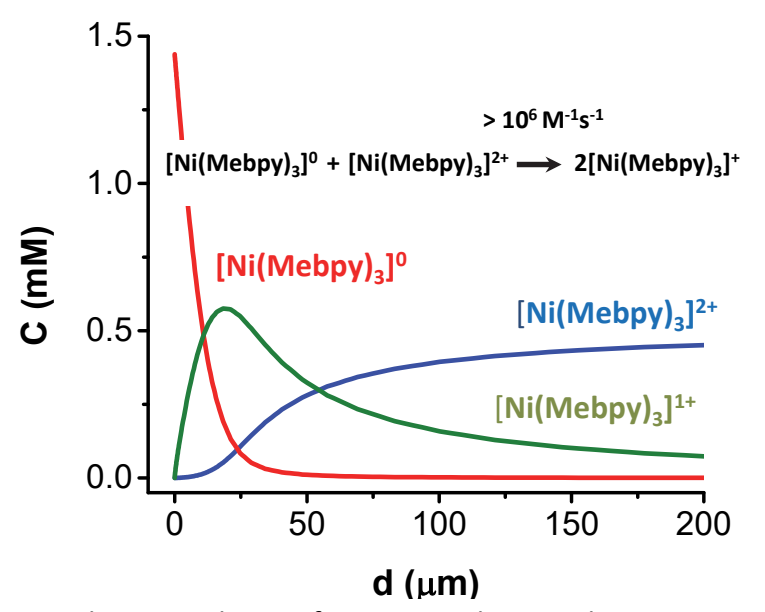
The authors would like to thank the CCI NSF Synthetic Organic Electrosynthesis Center for funding (CHE-1740656). C.S. thanks the EU for Horizon 2020 Marie Skłodowska-Curie Fellowship (grant no. 789399).

## References

- [1] J. P. Collin, A. Jouaiti, J. P. Sauvage, *Inorg. Chem.* **1988**, *27*, 1986–1990.
- [2] P.-A. Jacques, V. Artero, J. Pecaut, M. Fontecave, *Proc. Natl. Acad. Sci. U. S. A.* **2009**, *106*, 20627–20632.
- [3] J. Song, E. L. Klein, F. Neese, S. Ye, *Inorg. Chem.* **2014**, *53*, 7500–7507.
- [4] J. A. Ramos Sende, C. R. Arana, L. Hernandez, K. T. Potts, M. Keshevarzk, H. D. Abruna, *Inorg. Chem.* **1995**, *34*, 3339–3348.
- [5] Y. Kawamata, J. C. Vantourout, D. P. Hickey, P. Bai, L. Chen, Q. Hou, W. Qiao, K. Barman, M. A. Edwards, A. F. Garrido-Castro, J. N. deGruyter, H. Nakamura, K. Knouse, C. Qin, K. J. Clay, D. Bao, C. Li, J. T. Starr, C. Garcia-Irizarry, N. Sach, H. S. White, M. Neurock, S. D. Minteer, P. S. Baran, J. Am. Chem. Soc. 2019, 141, 6392–6402.
- [6] R. J. Perkins, D. J. Pedro, E. C. Hansen, Org. Lett. 2017, 19, 3755-3758.
- [7] T. J. DeLano, S. E. Reisman, ACS Catal. 2019, 9, 6751-6754.
- [8] B. J. Henne, D. E. Bartak, *Inorg. Chem.* **1984**, *23*, 369-373.
- [9] R. Prasad, D. B. Scaife, J. Electroanal. Chem., 1977, 84, 373.

- [10] Y. G. Budnikova, D. G. Yakhvarov, V. I. Morozov, Yu. M. Kargin, A. V. Il'yasov, Yu. N. Vyakhireva, O. G. Sinyashin, *Russ. J. Gen. Chem.* **2002**, *72*, 168–172.
- [11] P. N. Bartlett, V. Eastwick-Field, *Electrochim. Acta* **1993**, *38*, 2515–2523.
- [12] C. P. Winlove, K. H. Parker, R. K. C. Oxenham, *J. Electroanal. Chem. Interfacial Electrochem.* **1984**, *170*, 293–304.
- [13] G. Denuault, M. V. Mirkin, A. J. Bard, J. Electroanal. Chem. 1991, 308, 27-38.
- [14] A. J. Bard, L. R. Faulkner, Electrochemical Methods: Fundamentals and Applications, 2nd Ed., Wiley, New York **2001**.
- [15] J. D. Norton, H. S. White, J. Electroanal. Chem. 1992, 325, 341-350.
- [16] C. Amatore, S. C. Paulson, H. S. White, J. Electroanal. Chem. 1997, 439, 173–182.
- [17] K. B. Oldham, J. Electroanal. Chem. 1988, 250, 1-21.
- [18] C. Amatore, B. Fosset, J. Bartelt, M. R. Deakin, R. M. Wightman, *J. Electroanal. Chem. Interfacial Electrochem.* **1988**, *256*, 255–68.

# **Table of Contents Graphic**



Dr. Koushik Barman, Prof. Martin A. Edwards, Prof. David P. Hickey, Dr. Christopher Sandford, Dr. Yinghua Qiu, Prof. Rui Gao, Prof. Shelley D. Minteer\*, Prof. Henry S. White\*

Electrochemical Reduction of [Ni(Mebpy)<sub>3</sub>]<sup>2+</sup>. Elucidation of the Redox Mechanism by Cyclic Voltammetry and Steady-State Voltammetry in Low Ionic Strength Solutions

Bipyridine complexes of Ni are used as catalysts in a variety of reductive electrochemical and chemical transformations, where the Ni oxidation state and degree of ligation can dictate the catalytic pathway, efficacy, and selectivity.